# Analysis and Design of Flexible-Surface Induction-Heating Cooktop With GaN-HEMT-Based Multiple Inverter System

Eunsu Jang, Man Jae Kwon, *Student Member, IEEE*, Sang Min Park, Hyo Min Ahn, *Member, IEEE*, and Byoung Kuk Lee, *Senior Member, IEEE*

***Abstract*—The flexible induction cooktop, which can provide an unlimited cooking area, utilizes a cost-effective method in which one inverter shares multiple working coils. However, this method has resulted in consumer needs such as reducing both the initial pot detection time and the noise caused by the relay operation. This article presents a hardware implementation and control method for a flexible induction cooktop with multiple GaN-HEMT-based inverter systems. As one way to meet consumer needs, this implementation method does not require a relay and offers the advantage of real-time pot detection and noise minimization. However, the inverter design should include the magnetic coupling effect while maintaining high performance and high power density. This article proposes an inverter design method considering the limited space and an implementation method that minimizes the effect of magnetic coupling without an additional power stage. The feasibility of the proposed implementation method is evaluated based on the results of a heating test with a 3.3 kW prototype.**

***Index Terms*—Flexible-surface induction cooktop, induction heating (IH), multiple inverters, series resonant converter.**

## I. Introduction

THE induction heating (IH) cooktop has advantages such as fast heating time, safety, and ease of maintenance. Owing to these advantages, more IH cooktops are actively being produced and distributed to households instead of gas cooktops [1]–[10]. Most conventional IH cooktops are limited by their inability to heat pots made of nonferromagnetic materials. However, considering that most Asian household pots are made from nonferromagnetic materials such as aluminum and copper, an all-metal IH cooktop that can be heated regardless of the pot material is now in production [11]–[13]. Although the all-metal IH cooktop has solved the pot material limitation issue, the IH cooktop design still operates by using two to five working coils of assorted sizes, as shown in Fig. 1. This design limits the number of pots that can be heated at the same time and results in a low IH cooktop surface area utilization. To solve these problems, a flexible-surface IH cooktop with dozens of small working coils that can maximize the surface area utilization of the IH cooktop and simultaneously heat several pots has been developed (see Fig. 2) [14]–[20].

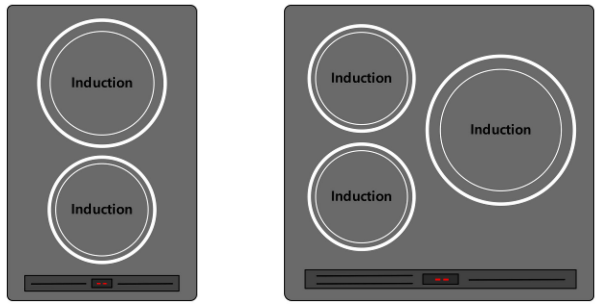


Fig. 1. Various types of commercial IH cooktop appliance. (a) Block diagram. (b) Inverter-coil integrated power unit.

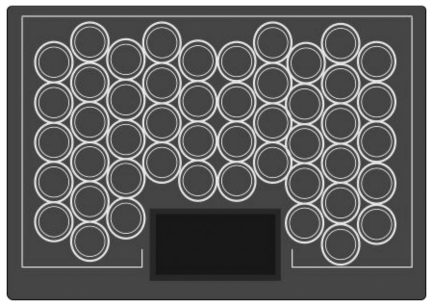

Fig. 2. IH cooktop appliance with multicoil.

Most flexible-surface IH cooktop systems on the home appliance market have a general structure in which one inverter shares several working coils through a relay, as shown in Fig. 3 [15]–[17]. This structure is cost effective as only two or four inverters can control dozens of working coils. However, this

Manuscript received December 15, 2021; revised March 3, 2022 and April 8, 2022; accepted May 10, 2022. Date of publication May 20, 2022; date of current version June 24, 2022. This work was supported in part by the Korea Institute of Energy Technology Evaluation and Planning and in part by the Ministry of Trade, Industry, and Energy of the Republic of Korea under Grant 20212020800020. Recommended for publication by Associate Editor J. Acero. *(Byoung Kuk Lee contributed equally to this work.) (Corresponding author: Byoung Kuk Lee.)*

Eunsu Jang, Man Jae Kwon, and Byoung Kuk Lee are with the Department of Electrical and Computer Engineering, Sungkyunkwan University College of Information and Communication Engineering, Suwon 16677, South Korea (e-mail: jespro@skku.edu; akswo1234@skku.edu; bkleeskku@skku.edu).

Sang Min Park is with the Korea Electronics Technology Institute, Bucheon 14502, South Korea (e-mail: smpark@keti.re.kr).

Hyo Min Ahn is with the Samsung Electronics, Suwon 16677, South Korea (e-mail: hyomin.ahn@samsung.com).

Color versions of one or more figures in this article are available at https://doi.org/10.1109/TPEL.2022.3175979.

Digital Object Identifier 10.1109/TPEL.2022.3175979

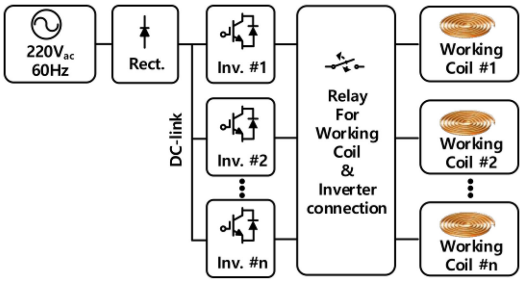


Fig. 3. Block diagram of conventional flexible-surface IH cooktop systems.

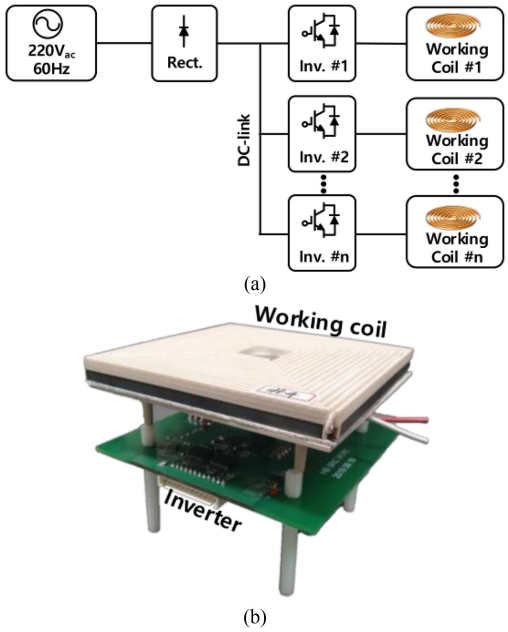


Fig. 4. Proposed inverter-coil integrated flexible-surface IH cooktop systems. (a) Block diagram. (b) Inverter-coil integrated power unit.

structure requires an additional circuit to detect the pot in real time. Because the inverter and the working coils are connected through a mechanical device such as a relay, a time delay, and mechanical noise may occur when forming the unit burner.

To solve this problem, a GaN-based inverter-coil integrated flexible-surface IH cooktop system in which the inverter and the working coil are individually matched has been proposed [21]. Since a relay used in a conventional system is not applied, inverter-coil integrated system alleviates both the time delay and mechanical noise problems. In addition, since each inverter can be operated at low power for pot detection, an additional pot detection circuit is not necessary. Moreover, the design of the inverter and the working coil as an integrated unit provides the convenience of easily replacing the faulty inverter-working coil unit.

However, although the GaN device ensures the high frequency and high power density design of the inverter-coil integrated unit, and can reduce the production costs by reducing the number of turns of the working coil, [21] still requires a large number of turns because a circular working coil structure with a small diameter of 70–80 mm is applied.

To increase the efficiency of the small size coil-based system and reduce total number of working coils, in [22] and [23], IH cooktops with overlapping working coils were presented. According to [22] and [23], the production cost was reduced compared to the conventional flexible surface IH cooktop by increasing the working coil area, and the energetic efficiency increased by about 1%. However, these structures may increase the control complexity by different distance to the load, and the constructive complexity of the working coil.

Moreover, in [21], an additional dc–dc for dc-link variable control is employed between the diode rectifier and the inverter. The dc–dc converter allows the inverter to operate close to the resonant frequency and provides high efficiency. However, the transient status of variable dc-link voltage control according to various load condition decides the boiling speed and transient response time of load variation. In addition, the additional dc–dc converter causes to reduce power density and entire efficiency and to increase entire manufacturing cost. Therefore, this article deals with the inverter-coil integrated flexible surface IH cooktop to which the power stage configuration of the conventional IH system is applied without a dc–dc converter, as shown in Fig. 4. Inverter-coil integrated units control the entire IH system with the proposed control algorithm instead of the dc–dc converter in [21], thus, the proposed IH system enhances the entire performance with respect of power density, efficiency, and transient response. Moreover, the number of turns of the working coil is reduced to 15 turns.

Studies on the power stage configuration and control algorithm of flexible surface IH cooktop have been conducted for the past several years. However, based on the previous studies, the additional considerations for the proper design of the inverter-coil integrated flexible surface IH cooktop are as follows:

1) optimal working coil shape design to maximize the utilization of cooktop surface area;
2) printed circuit boards (PCB) design for wide band gap (WBG) devices considering high-power-density and stray inductance [21], [24]–[29];
3) analysis of magnetic phenomena through FEM simulation [30]–[37].

Therefore, this article provides detailed design guidelines for the inverter-coil integrated IH cooktop from the hardware and control point of view. The heating performance of the designed system is evaluated using a 3.2 kW test bed under various conditions, and the proposed hardware implementation and control method are validated.

## II. Design of Flexible-Surface IH System

### A. Design of Working Coil

Each inverter is located at the bottom of the working coil. Therefore, the shape and size of the working coil determines the area utilization, the size and number of PCB, and the number of pots that can be detected and heated.

To determine the shape and size of the working coil, a built-in flexible-surface IH system with an $810 \times 520$ mm plate area was selected. Fig. 5 shows examples of working coils designed with assorted sizes and shapes within a limited area. The shape of the working coil may be circular, rectangular, or square among

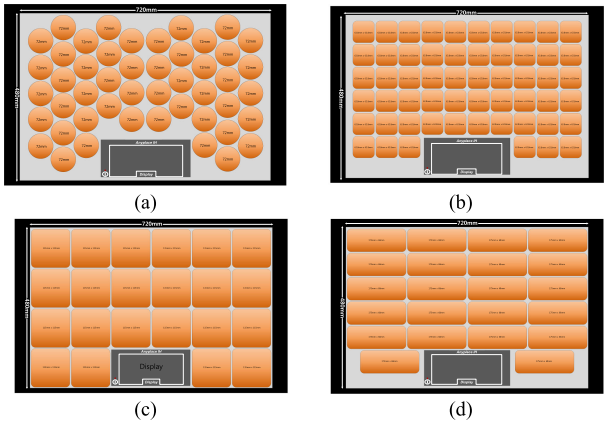


Fig. 5. Module structures of inverter and working coil. (a) Case 1. (b) Case 2. (c) Case 3. (d) Case 4.

TABLE I
SUMMARY OF CHARACTERISTICS ACCORDING TO WORKING COIL SHAPE

| | Case 1 | Case 2 | Case 3 | Case 4 |
|---|---|---|---|---|
| Shape | Circle | Square | Square | Rectangle |
| Size | Φ = 72 mm | 63.8×63.8 mm$^2$ | 115×115 mm$^2$ | 175×68 mm$^2$ |
| Count | 48 EA | 56 EA | 22 EA | 22 EA |
| Total coil area | 1954 cm$^2$ | 2280 cm$^2$ | 2909 cm$^2$ | 2677 cm$^2$ |
| Area utilization | 61.6% | 71.87% | 90.63% | 81.55% |

∗Area utilization = Total coil area / plate area × 100
∗Equal spacing between working coils = 3 mm

various other shapes. Table I summarizes the characteristics of each working coil shape shown in Fig. 5.

The empty space (dead zone) between the working coils increases as the diameter increases in circular working coils. Because this space cannot transfer power to the pot, it also makes it difficult to detect and heat pots smaller than 90 mm. Therefore, it is advantageous for circular working coils to have a diameter less than 100 mm. In contrast, for square and rectangular working coils, the dead-zone between working coils can be eliminated. To develop a unit burner that simultaneously heats one pot with multiple working coils, it is advantageous to increase the number of smaller working coils. However, because each inverter is located at the bottom of the working coil, the size of the PCB should also be considered. Moreover, when designing the area and number of working coils, the heating performance and cost efficiency with respect to the increase in the number of inverters and the miniaturization of working coils should be considered [15]. Therefore, Cases 1 and 2 are not suitable for the flexible-surface IH cooktop. The area-utilization rate of a rectangular working coil is approximately 10% lower than that of a square working coil, and its relatively long length (175 mm) increases the probability that two or more pots will be located on a single working coil. When two or more pots are placed on one working coil, the power for each pot cannot be controlled. Therefore, based on the analysis results of each working coil, the shape and size in Case 3 that would afford the densest use of the cooking surfaces were selected and designed.

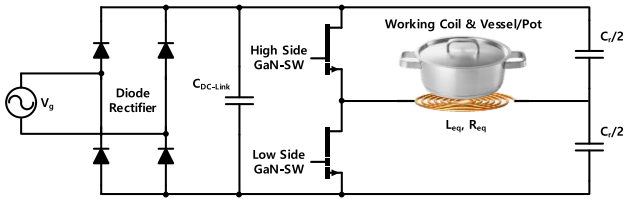


Fig. 6. Schematic of flexible-surface IH system.

TABLE II
COMPARISON AND ANALYSIS OF CHARACTERISTICS ACCORDING TO PCB POWER LOOP [26]

| Power loop | Lateral | Vertical | Optimal (Lateral and Vertical) |
|---|---|---|---|
| Single Sided PCB Capability | O | X | O |
| Field Self Cancellation | X | O | O |
| Inductance Independent of Board Thickness | O | X | O |
| Shield Layer Required | O | X | X |

### *B. Power Conversion System Using GaN-HEMT*

The entire flexible-surface IH system consists of a diode rectifier, IH inverters in a half-bridge series resonant converter topology, and working coils, as shown in Fig. 6 [21], [38], [39].

Based on the analysis results in Table I, the area of the PCB allocated to each IH inverter is 115 × 115 mm. Thus, it is advantageous to apply WBG devices such as SiC and GaN-HEMT to implement a high-power density design for the high-performance operation of inverters within a limited space. In particular, GaN-HEMT devices in the PQFN 8 × 8 package family are suitable for high-power density designs owing to characteristics such as a low volume and high switching performance. Therefore, LMG3410R050 from Texas Instruments was used to design IH inverters in this article.

The high dv/dt and di/dt, owing to the high-speed switching, cause an interaction between the parasitic components in the circuit and the switching device. In particular, a GaN-HEMT with a reduced threshold voltage ($V_{\rm th}$) and input capacitance ($C_{iss}$) can cause an unwanted turn-ON due to this interaction [27]. The LMG3410R050 device provides a pin to adjust the drain slew rate. Therefore, it is necessary to properly adjust the drain slew rate to prevent unwanted turn-ON owing to the high dv/dt. In addition, a PCB layout design that minimizes the stray inductance ($L_s$) should be considered to prevent gate ringing problems and unwanted turn-ON by di/dt. Recently, with the development of WBG devices, PCB layouts to reduce $L_S$ have been reviewed [26], [27]. Table II shows that the optimal power loop layout combines the advantages of lateral loops and vertical loops [26]. When applying the optimal power loop mentioned in Table II, it is possible to effectively reduce $L_S$ in a limited space through magnetic flux cancellation between PCB layers without a shield layer. Moreover, $L_s$ can be reduced by connecting capacitors in parallel close to the half-bridge leg or by increasing the copper width of the layer. Therefore, the PCB

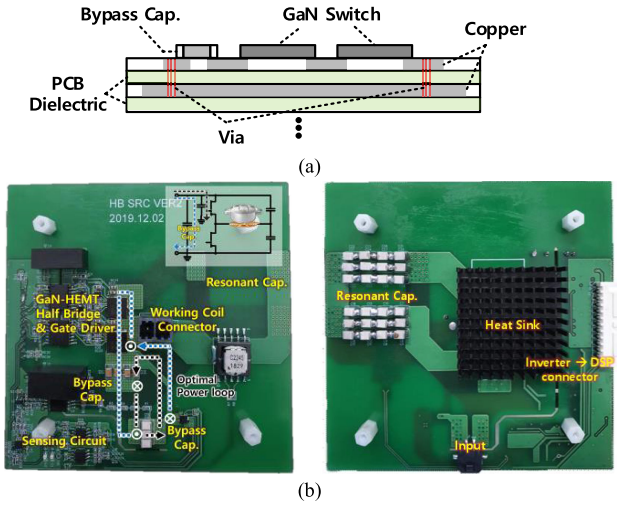


Fig. 7. PCB layout design. (a) PCB layout with optimal power loop. (b) Designed PCB layout.

layout was designed with the optimal power loop in Table II, as shown in Fig. 7(a), through the bypass capacitor. The designed PCB layout is shown in Fig. 7(b).

### C. Resonant Network Design for Each IH Inverter

Owing to the working coil conditions designed in Section II, the rated power of each IH inverter is limited. In this article, considering the 3.2-kW prototype, the rated power of each IH inverter ($P_{\mathrm{rate/coil}}$) was set to 800 W. Therefore, the resonant network had to be designed to satisfy the $P_{\mathrm{rate/coil}}$ within a limited area condition.

The working coil and pot can be modeled with an equivalent resistance and inductance ($R_{eq}$-$L_{eq}$) series circuit. Therefore, to satisfy the $P_{\mathrm{rate/coil}}$, the number of turns of the working coil should be designed to satisfy a value within the maximum impedance of the resonant network ($Z_{\max}$), which can be calculated as follows:

$$Z_{\max} = \frac{\left(\sqrt{2}V_{\mathrm{rms}}/\pi\right)^2}{P_{\mathrm{rate/coil}}} = \sqrt{{R_{eq}}^2 + \left(X_{Leq} - X_{Cr}\right)^2} \quad (1)$$

where $X_{Leq}$ is the inductive reactance of $L_{eq}$ and $X_{cr}$ is the capacitive reactance of $C_r$. As the impedance of the designed resonant network approaches the value calculated through (1), the magnitude of reactive power and the resonant current decrease. In this article, the switching frequency ($f_{\mathrm{sw}}$) range of the IH inverter is selected as 350–500 kHz in consideration of the limited space condition allocated to each IH inverter, the power loss and volume reduction rate due to the $f_{\mathrm{sw}}$ increase. Considering the selected frequency range, the working coil is optimized as follows: Under the input voltage condition of 220 $V_{\mathrm{rms}}$, $Z_{\max}$ calculated through (1) is about 6.5 Ω, and the rated current of IH inverter is calculated as 12–15 $A_{\mathrm{rms}}$. Therefore, 0.06 mm 360 strands of Litz-wire were selected considering the $f_{\mathrm{sw}}$ range of 350–500 kHz and its current rating. In addition, the number of turns of the working coil is set as one layer of 15 turns to satisfy $Z_{\max}$ in the $f_{\mathrm{sw}}$ range of 350–500 kHz. Moreover,

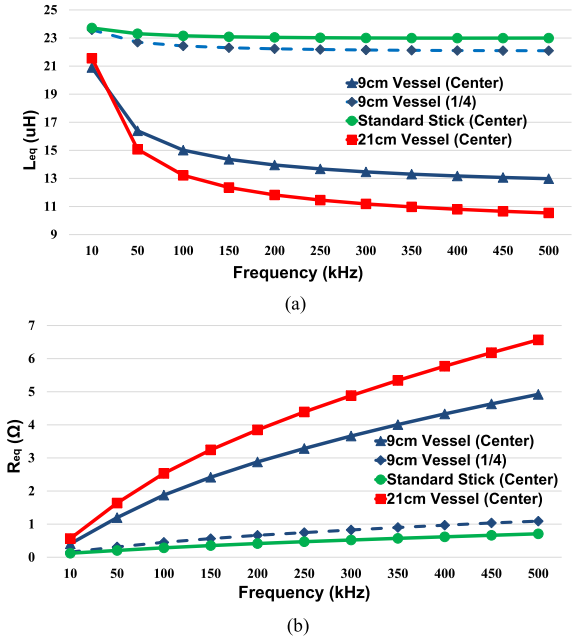


Fig. 8. Equivalent parameters depending on pot size and $f_{\mathrm{sw}}$. (a) $L_{eq}$. (b) $R_{eq}$.

a ferrite layer is applied to the bottom of each working coil to increase load coupling.

The parameters $R_{eq}$ and $L_{eq}$ of designed working coil are measured according to the various sizes of the pot, the occupancy of the working coil, and $f_{\mathrm{sw}}$, as shown in Fig. 8. The maximum $f_{\mathrm{sw}}$ (start frequency for soft start) is designed to be 500 kHz. Therefore, $C_r$ is designed to satisfy $P_{\mathrm{rate/coil}}$ in the frequency range of 350–500 kHz, through (2); its value is determined to be 14 nF, considering the average of the different $L_{eq}$ values in Fig. 8

$$C_r = \frac{1}{4\pi^2 {f_r}^2 L_{eq}}. \quad (2)$$

## III. Effects of Magnetic Coupling

When the magnetic flux generated by adjacent working coils is linked to other working coils, an electromagnetic force (EMF) is induced, causing difficulties in the power control of inverters. Magnetic coupling can increase the stress acting on the devices and damage the components in the inverter. For the magnetic coupling analysis, it is assumed that there are two adjacent IH inverters, as shown in Fig. 9(a). It is also assumed that these two IH inverters share one dc link with a constant voltage $V_d$ and operate at the resonant frequency ($f_r$). If the mutual coupling ($M$) is neglected, the impedance of the resonant circuit ($Z_{r,1}$), voltage ($v_1(t)$), and the resonant current ($i_{r,1}(t)$) of IH inverter 1 in Fig. 9(b) can be, respectively, expressed as

$$Z_{r,1} = R_{eq,1} + sL_{eq,1} + \frac{1}{sC_r} \quad (3)$$

$$v_1(t) = \frac{4V_d}{\pi}\sin\omega t \quad (4)$$

$$i_{r,1}(t) = \frac{v_1(t)}{Z_{r,1}} = \frac{4V_d}{Z_{r,1}\pi}\sin\omega t. \quad (5)$$

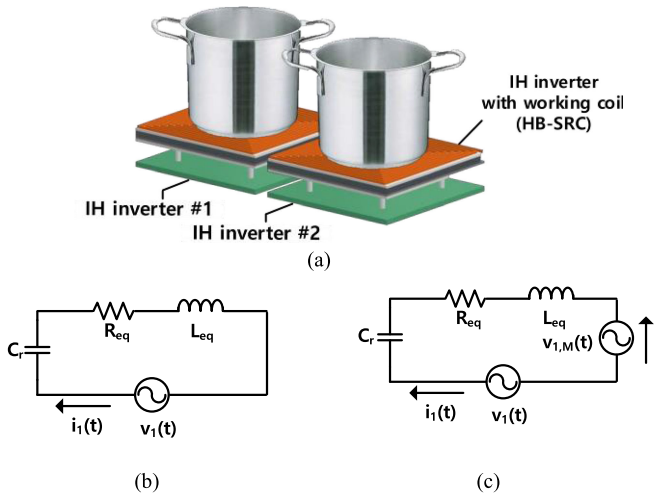


Fig. 9. Equivalent circuit according to magnetic coupling. (a) Proposed IH system structure. (b) Equivalent circuit without magnetic coupling. (c) Equivalent circuit with magnetic coupling.

Assuming that two IH inverters operate at the same frequency and that the voltage phase angle between them is $\theta$, the voltage ($v_2(t)$) and resonant current ($i_{r,2}(t)$) of IH inverter 2 can be calculated as follows:

$$v_2(t) = \frac{4V_d}{\pi}\sin(\omega t - \theta) \tag{6}$$

$$i_{r,2}(t) = \frac{v_2(t)}{Z_{r,2}} = \frac{4V_d}{Z_{r,2}\pi}\sin(\omega t - \theta) \tag{7}$$

where $Z_{r,2}$ is the impedance of the resonant circuit of IH inverter 2. When $M$ is considered, the EMF induced in IH inverter 1 ($v_{1,M}$) by the magnetic flux generated in the working coil of IH inverter 2 in Fig. 9(c) can be obtained as follows:

$$\begin{aligned} v_{1,M}(t) &= R_M i_{r,2}(t) \pm M\frac{di_{r,2}(t)}{dt} \\ &= \sqrt{2}R_M I_{r,2}\sin(\omega t - \theta) \pm \sqrt{2}\omega M I_{r,2}\cos(\omega t - \theta) \end{aligned} \tag{8}$$

where $I_{r,2}$ is rms value of $i_{r,2}(t)$ and $R_M$ is the mutual resistance. Owing to the high-frequency operation of the IH inverter ($R_M \ll \omega M$), (8) can be rewritten considering only $v_{12,M}(t)$ caused by $\omega M$, as follows [31]:

$$v_{1,M}(t) = M\frac{di_{r,2}(t)}{dt} = \sqrt{2}\omega M I_{r,2}\cos(\omega t - \theta). \tag{9}$$

$v_1(t)$, considering (9), can be defined as follows:

$$v_1(t) = \frac{4V_d}{\pi}\sin\omega t \pm v_{1,M}. \tag{10}$$

The magnetic flux density was estimated using finite element analysis (FEM) simulation. The detailed configuration of FEM simulation is shown in Fig. 10, and the simulation results are shown in Fig. 11. Simulation results were analyzed to determine the effect of increasing $\theta$ under the conditions 0, $\pi/4$, $\pi/2$, and $2\pi/3$, respectively. As shown in Fig. 11(a)–(d), the magnetic flux generated in the working coils is inclined horizontally as $\theta$ increases. In particular, as $\theta$ increases the magnetic flux in

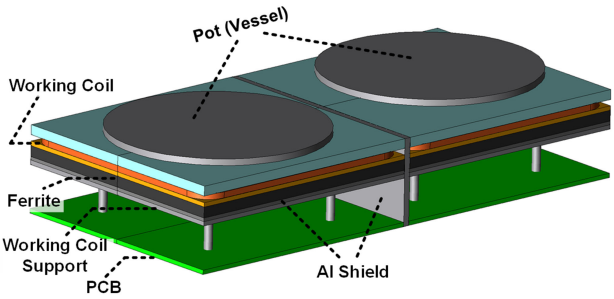


Fig. 10. Schematic of FEM simulation.

the space between the working coils is oriented from the top of the working coil to the ferrite direction of the working coil (i.e., ferrite of the corresponding or adjacent working coil), and as can be inferred from the simulation results, magnetic coupling occurs mainly in this space and increases the EMF which can be calculated using (9). When the distance between the working coils is fixed at 3 mm, the most effective method of minimizing the influence of the magnetic coupling is to shield the space where magnetic coupling occurs. Fig. 11(e)–(h) shows the magnetic flux density when an Al shield is placed in the space between the working coils. By shielding the space where magnetic coupling occurs through an Al shield, the induced EMF can be reduced. Based on the FEM simulation results $v_1(t)$ according to the aluminum (Al) shield is calculated. When each IH inverter operates under different $\theta$ and same $f_{\mathrm{sw}}$ conditions, $v_1(t)$ is calculated as shown in Fig. 12(a)–(c). On the other hand, Fig. 12(d)–(e) shows the condition of different $f_{\mathrm{sw}}$. As shown in these Fig. 12(a)–(c), when the phase angle is different, $v_1(t)$ becomes reduced because negative EMF become increased. In this condition, these phenomena become enhanced by inserting Al shield. In case that $f_{\mathrm{sw}}$ of the adjacent inverters are different, as shown in Fig. 12(d)–(e), $v_1(t)$ becomes fluctuated due to the different generation aspect of EMF of each coil according to different frequencies. However, this phenomenon is also enhanced by inserting Al shield. Moreover, when the frequency of the resonant current flowing in the adjacent working coil are different, as shown in Fig. 12(d), acoustic noise corresponding to the frequency difference of each resonant current is generated. For example, when IH inverter 1 operates at an operating frequency of 400 kHz, and IH inverter 2 operates at 405 kHz, an acoustic noise of 5 kHz corresponding to the frequency difference of the resonant current is generated. However, in a flexible-surface IH system with multiple inverters, it is difficult to synchronize the pulsewidth modulation ON/OFF of all inverters corresponding to the unit burner. Therefore, hardware implementation or control methods such as Al shield should be applied to flexible-surface IH in consideration of the influence of magnetic coupling.

Verification tests were performed at low power levels of 100 W or less. The test results with and without Al shield are as follows. When $\theta = 0$, the input power remains constant with or without an Al shield. In contrast, for $\theta = \pi$, since $v_1(t)$ decreases owing to magnetic coupling, the input power is reduced by up

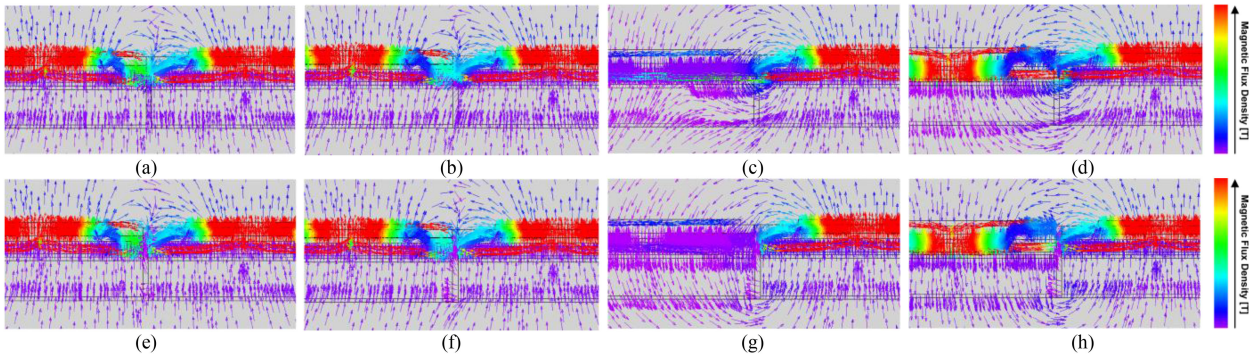


Fig. 11. FEM simulation results according to $\theta$ and Al shield. (a) w/o Al shield, $\theta$=0. (b) w/o Al shield, $\theta$= $\pi$/4. (c) w/o Al shield, $\theta$= $\pi$/2. (d) w/o Al shield, $\theta$= 2$\pi$/3. (e) w/ Al shield, $\theta$=0. (f) w/ Al shield, $\theta$= $\pi$/4. (g) w/ Al shield, $\theta$= $\pi$/2. (h) w/ Al shield, $\theta$= 2$\pi$/3.

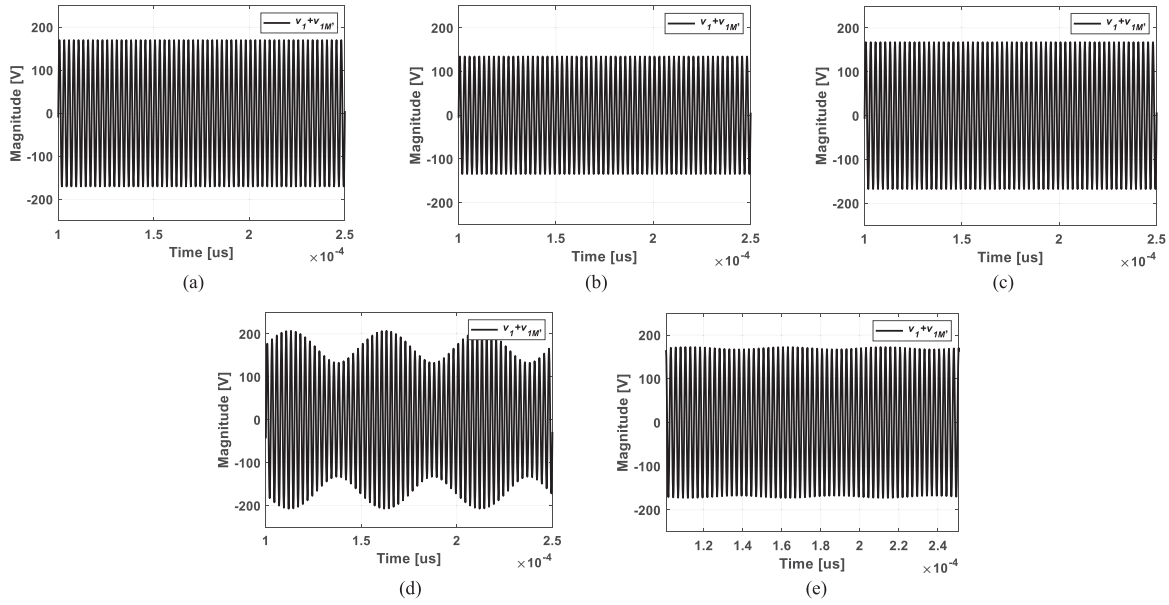


Fig. 12. EMF according to the $\theta$ and $f_{\mathrm{sw}}$. (a) Same $f_{\mathrm{sw}}$, $\theta$=0. (b) Same $f_{\mathrm{sw}}$, $\theta$=$\pi$/2, w/o Al shield. (c) Same $f_{sw}$, $\theta$=$\pi$/2, w/ Al shield. (d) 20 [kHz] of $f_{\mathrm{sw}}$ difference (w/o Al shield). (e) 20 [kHz] of $f_{\mathrm{sw}}$ difference (w/ Al shield).

to 24.3% when the Al shield is not applied, compared with that under the condition with the Al shield. However, when the Al shield is applied, the input power is reduced by up to 9.4%. Therefore, the effect of EMF is significantly improved compared with when the Al shield is not applied. Moreover, it was verified that acoustic noise was reduced when the Al shield was applied, even under the rated power condition. As a result, when the Al shield is applied, it can be confirmed that flexible-surface IH can be implemented without requiring an additional power stage or control method.

## IV. Control Algorithm for Flexible-Surface IH System

This section presents control algorithms for implementing the flexible-surface IH, including the identification of pots and foreign objects, such as spoons and chopsticks, movement detection during pot heating, unit burner formation, and frequency synchronization. Each IH inverter implements flexible-surface IH by communicating via a control area network (CAN) with the main microcontroller unit (MCU). Through the CAN, master and slave MCUs share information on the status and location of pots, input power, operating frequency, reference power, reference frequency, and trip status.

### A. Identification of Pots, Foreign Objects, and Unit Burner Formation

The initial algorithm for identifying pot and foreign object is based on the input power measured by the corresponding inverter when the pot is placed on the working coil. Power losses owing to continuous pot detection operation can be reduced by applying pulse density modulation control, and the input power for pot detection is not high enough to heat the foreign object. Each inverter in the flexible-surface IH system performs a soft start at an initial operating frequency of 500 kHz. The input power is measured differently according to the load condition (pot size) and can be divided into no-load, foreign object level, small pot ($<$ 100 mm), and large pot ($\geq$ 100 mm) groups using the curve-fitting method (CFM), as shown in Fig 13. The size of a standard

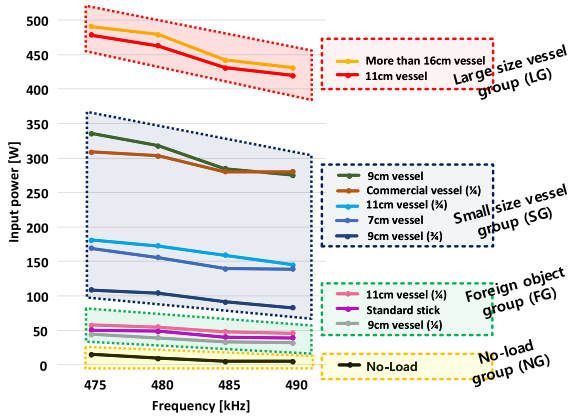


Fig. 13. Input power according to pot occupied area.

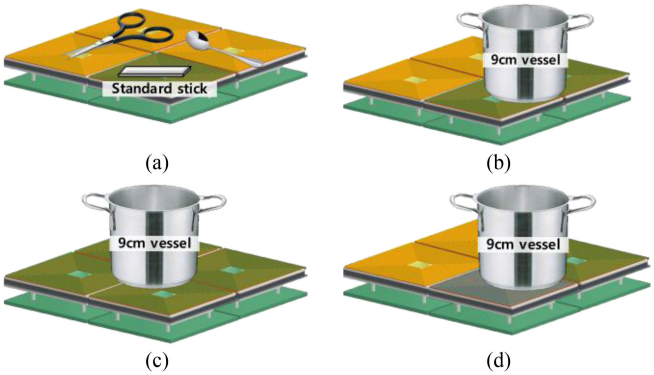


Fig. 14. Difficulty of control depending on the pot position. (a) Standard stick. (b) 9 cm pot 1/2;. (c) 9 cm pot 1/4;. (d) 9 cm pot 3/4 and 1/4.

stick is defined in the IEC 60335-2-9 standard (20 × 100 mm); foreign objects smaller than the standard stick are considered to be no-load and are not heated [38].

The no-load group status (NG) is identified because the input power is small. In addition, by setting the upper and lower limits of the input power, the foreign-object group status (FG) and small and large pot group statuses (SG and LG) can be identified. However, some conditions make it difficult to identify the pot state, as shown in Fig. 14(a)–(d).

1) Conditions in which only one of the adjacent IH inverters is identified as FG status: Identification as NG status by the prefitted power curve (nonoperation).
2) Conditions in which two or more adjacent IH inverters are identified as FG status: Identified as the smallest-size (90 mm) pot by the prefitted power curve (operation). In fact, when kitchen utensils such as spoons, scissors, and knives are placed between two or more working coils, the input power measured by the IH inverter is as low as that for the NG status, as shown in Fig. 14(a). Moreover, because the designed working coil area is large, when adjacent IH inverters simultaneously measure the input power within the FG level, this implies that a small pot is occupying several working coils, as shown in Fig. 14(b).
3) Condition in which four or more adjacent IH inverters are identified as FG status: Identified as a small pot occupying more than four working coils, by using the prefitted power curve, as depicted in Fig. 14(c)(operation).
4) Conditions in which two or more adjacent IH inverters are identified simultaneously as FG and SG: One or more small (or large) pots are identified as occupying multiple working coils. In this case, the flexible-surface IH system operates under two scenarios depending on the needs of the user.
   a) When the user needs to heat adjacent pots with different input powers, the main MCU transmits different target power values to each IH inverter. Even though the IH inverters operate at different frequencies, magnetic coupling and acoustic noise are reduced by the Al shield.
   b) In the condition shown in Fig. 15, Main MCU recognizes that four adjacent IH inverters detect the status of FG or SG. When the user needs to heat the pot by forming a unit burner, the main MCU configures corresponding IH inverters as unit burners. The main MCU composes the PI controller, as shown in Fig. 15, by summing the input power values of each IH inverter received in real time through CAN communication, where $P_{ref}$ in Fig. 15 is a preset value according to the heating level the user selects for heating. In addition, the output of the PI controller ($f_{\mathrm{sw}}$) is transmitted back to each IH inverter in real time through CAN communication so that the unit $f_{\mathrm{sw}}$ of the burner can operate in synchronization. At this time, each IH inverter outputs different power because the area occupied by the pot is different for each working coil. (If one IH inverter is identified as SG or higher, the pot can be heated using only one IH inverter.)

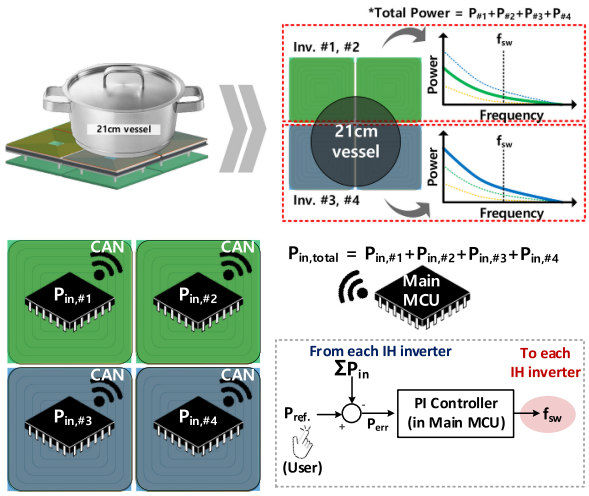


Fig. 15. Example of flexible surface IH control - condition (d)

To execute the previously-explained control methods, each IH inverter is assigned a respective number (e.g., #1, #2, #3, #4).

When the input power is below the SG level, the coupling degree between the pot and the working coil is too low, and the phase between the pole voltage and the resonant current increases. Moreover, owing to the decrease in $R_{eq}$, the resonant

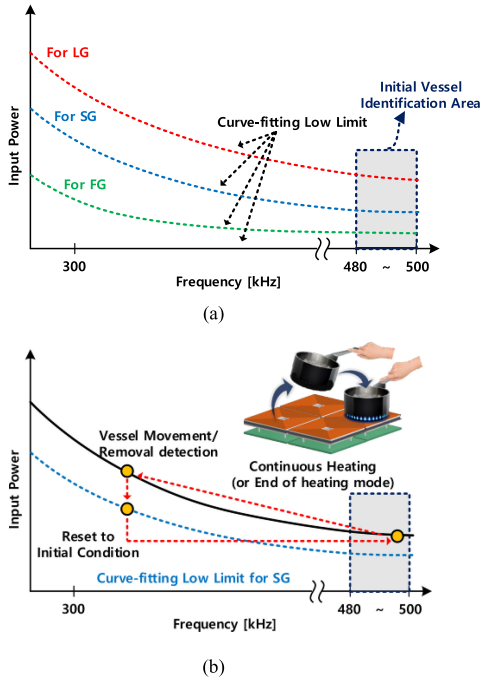


Fig. 16. CFM-based pot movement/removal detection algorithm. (a) Fitted power curve for each pot identification group. (b) Sequence of the control algorithm.

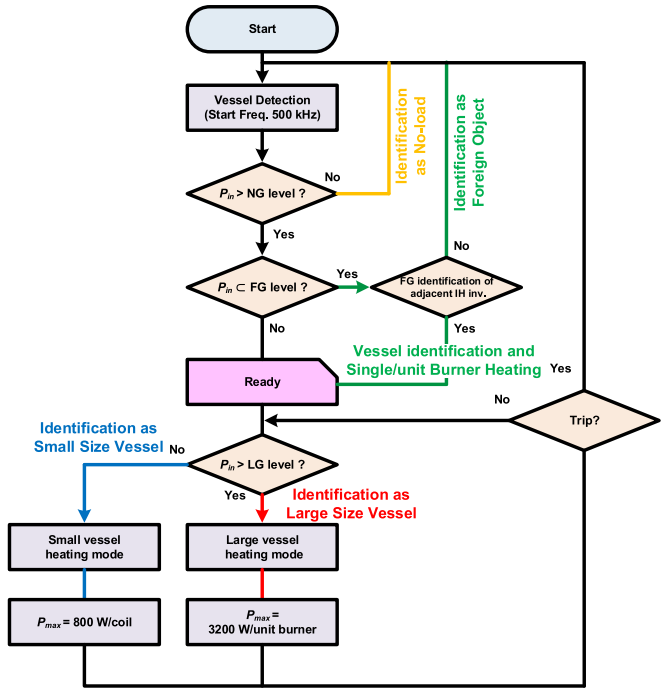


Fig. 17. Control block diagram of flexible surface IH.

current needed to satisfy the input power received from the main MCU to the IH inverter increases. In this case, the loss in the dead-time period increases owing to the high forward voltage ($V_f$) of the antiparallel diode of the GaN-HEMT. Therefore, when the input power is below the SG status, the rated output of each IH inverter is limited to 800 W.

### B. Movement Detection During Pot Heating

In an IH cooktop, when a pot moves or is removed during the heating operation, the control algorithm must quickly determine the pot location and decide whether to continue heating, reset the system, or turn OFF the power. Because the flexible-surface IH system has several IH inverters adjacent to each other, the movement of the pot should be determined even more quickly. In this article, movement detection control is performed through the CFM, as shown in Fig. 16(a). The operation methods can be explained through Fig. 16(b), as follows.

1) A decrease in the input power is detected depending on the change in working coil occupancy when moving the pot.
2) The measured input power value meets the prefitted minimum power curve.
3) The IH inverter operating frequency is changed to the initial state, and the target power value from the previous operation is maintained for several seconds in the main MCU.
4) If the adjacent IH inverter detects a pot of the same size within seconds, the slave inverters receive the reference power from the MCU and continuously heat the pot. However, if the pot is not detected, the inverter switches to the initial pot-detection mode.

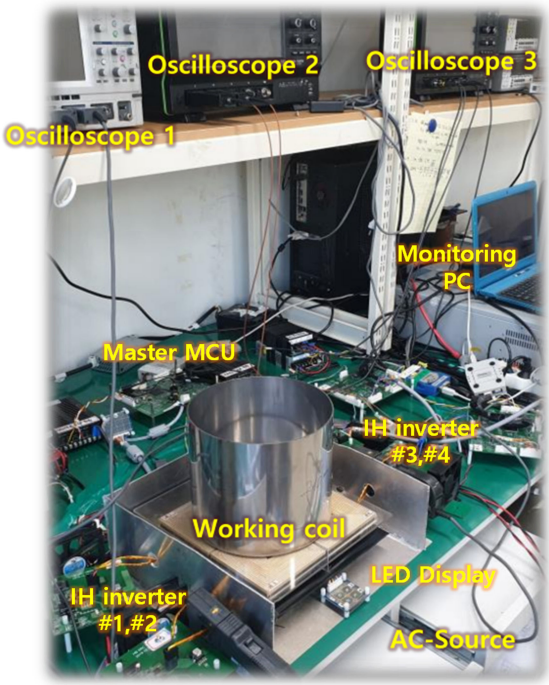


Fig. 18. 3.2 kW flexible surface IH prototype.

The overall control-block diagram of the flexible-surface IH system, including the control algorithms described previously, is summarized, as shown in Fig. 17.

## V. Experimental Verification

This section describes the evaluation results of the designed 3.2 kW flexible-surface IH system. At least four IH inverters are required to implement and verify the control algorithm

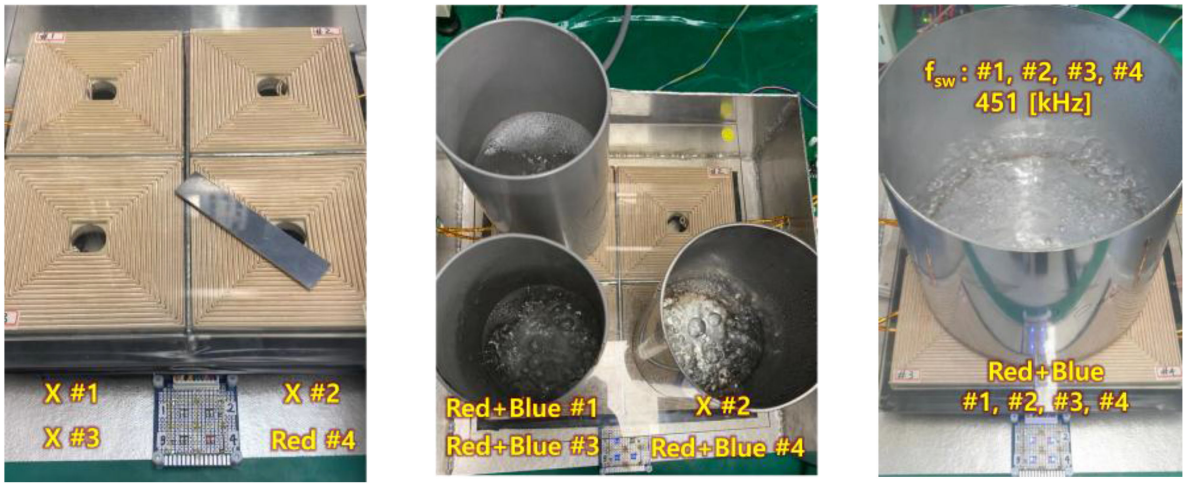


(a) (b) (c)

Fig. 19. LED display status according to pot position. (a) Standard stick. (b) Three small pots. (c) Large size (210 mm) pot.

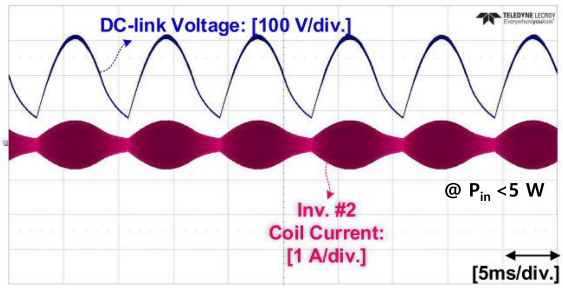


Fig. 20. Experimental waveform of IH inverter stage - Fig. 19(a) condition.

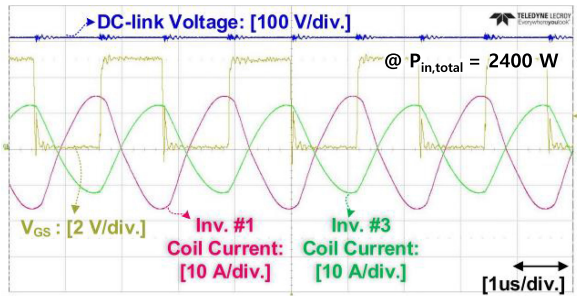


Fig. 21. Experimental waveform of IH inverter stage - Fig. 19(b) condition.

described in the previous section. Therefore, as shown in Fig. 18, experimental verification is performed with four IH inverters, one main MCU, a standard pot of each size, and an LED circuit for indicating the pot status. As previously mentioned, the rated power of each IH inverter is limited to 800 W under the SG status.

Fig. 19(a)–(c) shows that each IH inverter identifies the location and status of the pot in real time. The displayed color of the LED confirms the pot-identification status of each IH inverter. Only the red LED being displayed indicates that the IH inverter is identified as having the FG status of Fig. 13; when the red and blue LEDs are displayed simultaneously, the IH inverter is identified as SG or higher; When all LEDs of adjacent IH inverter units are displayed, it means that the IH inverter has identified as LG status in the unit burner condition.

Fig. 19(a) illustrates the foreign object detection, as shown in Fig. 14(a). As mentioned in the previous section, FG status has been identified by the prefitted power curve and the IH inverter cannot be operated. The experimental waveform of the condition of Fig. 19(a) is shown in Fig 20. The IH inverter detects a no-load condition and does not initiate the heating operation. In FG status, the input power is not high about around 3 W, so that the foreign object cannot be heated. Fig. 19(b) and (c) shows the conditions in which one or more IH inverters have been identified as having the SG or higher statuses by the prefitted power curve. From Fig. 19(b), it is evident that three adjacent IH inverters display red and blue LEDs. The main MCU is set up such that adjacent IH inverters heat the pot with different input power levels. Fig. 21 shows that each IH inverter satisfies the input power condition of 800 W at different $f_{\mathrm{sw}}$ depending on the pot material and location and performs stable heating operations.

In the condition of Fig. 19(b), when the Al shield was removed, the input power was reduced, a loud acoustic noise was caused by magnetic coupling, and some IH inverters were damaged. In addition, it was confirmed that when each IH inverter operates at different frequencies, current ringing corresponding to the operating frequency difference of each IH inverter occurs in the input current waveform, as shown in Fig. 22. However, when the Al shield was applied, the current ringing did not disappear completely, but the effect of magnetic coupling such as input power reduction was minimized, and the acoustic noise caused by the $f_{\mathrm{sw}}$ difference of the IH inverters was significantly reduced. It was confirmed that the IH inverter achieved stable operation without damage.

Fig. 19(c) shows the condition of heating one large pot by forming a unit burner. The four IH inverters operate under the same $f_{\mathrm{sw}}$ received from the main MCU. As mentioned in Fig. 15, the input power of each inverter differs depending on the area of the pot located over each working coil. Stable operation with a power factor (PF) of 0.99 under the unit burner condition was confirmed, as shown in Fig. 23.

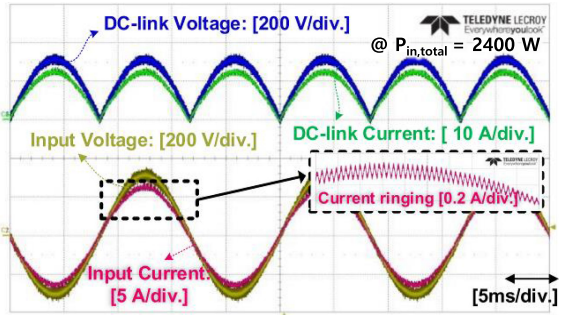


Fig. 22. Experimental waveform of rectifier stage w/o Al shield- Fig. 19(b) condition.

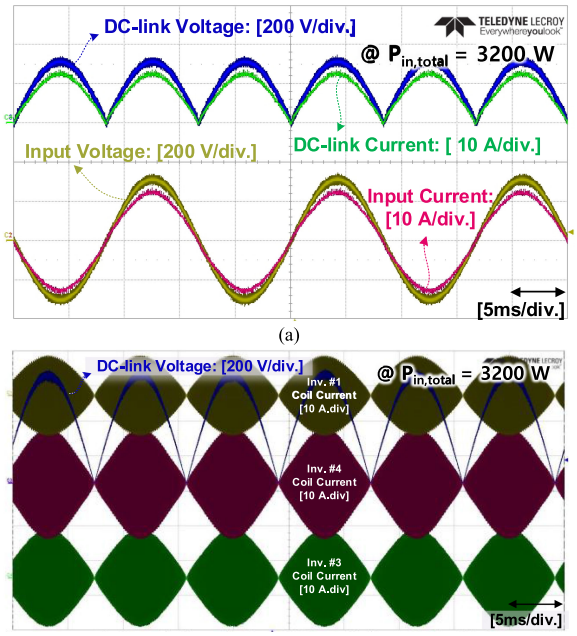


Fig. 23. Main experimental waveform - Fig. 18(c) condition. (a) Rectifier stage. (b) IH inverter stage.

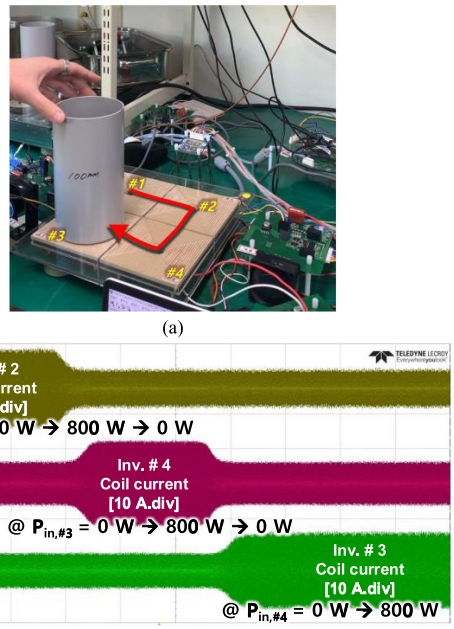


Fig. 24. Results of vessel movement/removal detection test. (a) Vessel movement direction. (b) Coil current waveform when moving vessel.

TABLE III
MEASUREMENT RESULT OF HEATING EFFICIENCY

| Pot Size | Amount of Water | Input Power | Mode | Heating Efficiency |
|---|---|---|---|---|
| 90 mm | 0.8 L | 800 W | Single | 93.49% |
| 160 mm | 1.5 L | 800 W | Single | 94.26% |
| 210 mm | 2.0 L | 1500 W | Unit Burner | 87.78% |

Fig. 24 shows the experimental results according to the change in pot position. When the pot is moved clockwise during heating operation, as shown in Fig. 24(a), the input power of the IH inverter, which was in heating operation, decreases, and meets the power curve fitted for reset, as shown in Fig. 16. Fig. 24(b) shows that the input power of the IH inverter is reset to the initial pot-identification state when it meets the prefitted power curve. In addition, when the pot is placed on another working coil, it can be confirmed that the corresponding IH inverter receives the previous target power value from the main MCU and continuously heats the pot. In this case, the input power changes only once when the pot is moved or removed, so that the pot movement does not affect to flicker emission mentioned in IEC standard 1000-3-3 [39], [40].

The heating performance of the designed flexible-surface IH system was verified through boiling efficiency calculated from measured heating time at rated power conditions, amount of water, weight, and specific heat of pot, according to the IEC 60335-2-9 standard [38]. Boiling efficiency measurements were performed under single IH inverter operating conditions and unit burner conditions. The experimental conditions, such as the pot size and amount of water used to measure boiling efficiency, as well as the experimental results, are listed in Table III. When heating the pot through one IH inverter, it was confirmed that the heating efficiency was as high as 94.26%, when the IH inverter operated close to the resonant frequency.

In addition, when heating a 210-mm pot using a unit burner, the heating efficiency of the flexible-surface IH system was measured to be a maximum of 87.78% because of the increase in the reactive power of each IH inverter due to the decrease in coupling between the pot and the working coil. Considering that the boiling efficiency of the IH cooktop on the market is around 90%, the results in Table III verify the high heating performance of the designed prototype in this article. In addition, the power stage efficiency of the prototype is 98%, which shows high efficiency even under high-frequency operating conditions of 350–500 kHz.

Moreover, through the heating test, it was confirmed that the proposed flexible-surface IH system satisfies the minimum PF 0.97 and maximum PF 0.99 under all heating conditions. Based on the heating efficiency of about 90% and the measured PF results, the high heating performance of the proposed structure was verified.

## VI. Conclusion

To solve the problems caused by magnetic coupling, a hardware implementation method and a control algorithm for a flexible-surface IH system were proposed in this article.

For high performance and a high-power density, a GaN-HEMT based inverter and a square working coil-based resonance network were designed. The validity of the proposed hardware implementation and control method was verified by confirming the reduction in the effects of magnetic coupling through the experimental results, based on a 3.2-kW prototype. Finally, the designed flexible-surface IH system was evaluated by measuring the heating efficiency. The maximum heating efficiency was confirmed to be 94.26% when operating a single IH inverter and 87.78% when operating a unit burner. The maximum PF was 0.99, and the high heating efficiency of the proposed structure was verified based on the experimental results.

## References


[1] O. Lucía, P. Maussion, E. J. Dede, and J. M. Burdío, "Induction heating technology and its applications: Past developments, current technology, and future challenges," *IEEE Trans. Ind. Electron.*, vol. 61, no. 5, pp. 2509–2520, May 2014.

[2] O. Lucia, J. Acero, C. Carretero, and J. M. Burdio, "Induction heating appliances: Toward more flexible cooking surfaces," *IEEE Ind. Electron. Mag.*, vol. 7, no. 3, pp. 35–47, Sep. 2013.

[3] J. Acero *et al.*, "The domestic induction heating appliance: An overview of recent research," in *Proc. 23rd Annu. IEEE Appl. Power Electron. Conf. Expo.*, Austin, TX, USA, 2008, pp. 651–657.

[4] V. Esteve *et al.*, "Using pulse density modulation to improve the efficiency of IGBT inverters in induction heating applications," in *Proc. IEEE Power Electron. Specialists Conf.*, Orlando, FL, USA, 2007, pp. 1370–1373.

[5] İ. Yılmaz, M. Ermiş, and I. Çadırcı, "Medium frequency induction melting furnace as a load on the power system," in *Proc. IEEE Ind. Appl. Soc. Annu. Meeting*, Orlando, FL, USA, 2011, pp. 1–12.

[6] J. Egalon, S. Caux, P. Maussion, M. Souley, and O. Pateau, "Multiphase system for metal disc induction heating: Modeling and RMS current control," *IEEE Trans. Ind. Appl.*, vol. 48, no. 5, pp. 1692–1699, Sep./Oct. 2012.

[7] Ó. Lucia, L. A. Barragán, J. M. Burdio, Ó. Jimenez, D. Navarro, and I. Urriza, "A versatile power electronics test-bench architecture applied to domestic induction heating," *IEEE Trans. Ind. Electron.*, vol. 58, no. 3, pp. 998–1007, Mar. 2011.

[8] H. Sarnago, A. Mediano, and Ó. Lucia, "High efficiency AC–AC power electronic converter applied to domestic induction heating," *IEEE Trans. Power Electron.*, vol. 27, no. 8, pp. 3676–3684, Aug. 2012.

[9] G. T. Landi and A. F. Bakuzis, "On the energy conversion efficiency in magnetic hyperthermia applications: A new perspective to analyze the departure from the linear regime," *J. Appl. Phys.*, vol. 111, no. 8, Apr. 2012, Art. no. 083915.

[10] C.-C. Tai and M.-K. Chen, "The design of a half-bridge series-resonant type heating system for magnetic nanoparticle thermotherapy," *PIERS Online*, vol. 4, no. 2, pp. 276–280, Jan. 2008.

[11] I. Millán, J. M. Burdío, J. Acero, O. Lucía, and S. Llorente, "Series resonant inverter with selective harmonic operation applied to all-metal domestic induction heating," *IET Power Electron.*, vol. 4, no. 5, pp. 587–592, May 2011.

[12] T. Tanaka, "A new induction cooking range for heating any kind of metal vessels," *IEEE Trans. Consum. Electron.*, vol. 35, no. 3, pp. 635–641, Aug. 1989.

[13] H. Park and J. Jung, "Load-Adaptive modulation of a series-resonant inverter for all-metal induction heating applications," *IEEE Trans. Ind. Electron.*, vol. 65, no. 9, pp. 6983–6993, Sep. 2018.

[14] H. Sarnago, Ó. Lucía, and J. M. Burdío, "FPGA-Based resonant load identification technique for flexible induction heating appliances," *IEEE Trans. Ind. Electron.*, vol. 65, no. 12, pp. 9421–9428, Dec. 2018.

[15] J. Serrano, J. Acero, I. Lope, C. Carretero, and J. M. Burdío, "A flexible cooking zone composed of partially overlapped inductors," *IEEE Trans. Ind. Electron.*, vol. 65, no. 10, pp. 7762–7771, Oct. 2018.

[16] H. Sarnago, P. Guillén, J. M. Burdío, and O. Lucia, "Multiple-Output ZVS resonant inverter architecture for flexible induction heating appliances," *IEEE Access*, vol. 7, pp. 157046–157056, 2019.

[17] J. Acero, C. Carretero, Ó. Lucía, R. Alonso, and J. M. Burdío, "Mutual impedance of small ring-type coils for multiwinding induction heating appliances," *IEEE Trans. Power Electron.*, vol. 28, no. 2, pp. 1025–1035, Feb. 2013.

[18] H. W. Koertzen, J. D. V. Wyk, and J. A. Ferreira, "Design of the halfbridge series resonant converters for induction cooking," in *Proc. IEEE Power Electron. Specialist Conf.*, 1995, pp. 729–735.

[19] M. Kamli, S. Yamamoto, and M. Abe, "A 50–150 kHz half-bridge inverter for induction heating applications," *IEEE Trans. Ind. Electron.*, vol. 43, no. 1, pp. 163–172, Feb. 1996.

[20] E. J. Dede, J. V. Gonzalez, J. A. Linares, J. Jordan, D. Ramirez, and P. Rueda, "25-kW/50-kHz generator for induction heating," *IEEE Trans. Ind. Electron.*, vol. 38, no. 3, pp. 203–209, Jun. 1991.

[21] H. Sarnago, J. M. Burdío, and O. Lucia, "High-Frequency gan-Based induction heating versatile module for flexible cooking surfaces," in *Proc. IEEE Appl. Power Electron. Conf. Expo.*, Anaheim, CA, USA, 2019, pp. 448–452.

[22] J. Serrano, J. Acero, I. Lope, C. Carretero, and J. M. Burdío, "A flexible cooking zone composed of partially overlapped inductors," *IEEE Trans. Ind. Electron.*, vol. 65, no. 10, pp. 7762–7771, Oct. 2018.

[23] J. Serrano, I. Lope, and J. Acero, "Nonplanar overlapped inductors applied to domestic induction heating appliances," *IEEE Trans. Ind. Electron.*, vol. 66, no. 9, pp. 6916–6924, Sep. 2019.

[24] T. Mishima, "Latest development of SiC power Module-based single-stage AC-AC resonant converter for high-frequency induction heating applications," in *Proc. Int. Power Electron. Conf.*, Niigata, Japan, 2018, pp. 872–877.

[25] M. Pérez-Tarragona, H. Sarnago, Ó. Lucía, and J. M. Burdío, "Full-bridge series resonant multi-inverter featuring new 900-V SiC devices for improved induction heating appliances," in *Proc. IEEE Appl. Power Electron. Conf. Expo.*, Long Beach, CA, USA, 2016, pp. 1762–1766.

[26] D. Reusch and J. Strydom, "Understanding the effect of PCB layout on circuit performance in a high-frequency gallium-nitride-based point of load converter," *IEEE Trans. Power Electron.*, vol. 29, no. 4, pp. 2008–2015, Apr. 2014.

[27] D. Joo, H. Kim, B. Lee, and J.-S. Kim, "Hardware implementation of GaN-HEMT based ZVS DC–DC converter considering PCB layout," *J. Elect. Eng. Technol.*, vol. 14, no. 5, pp. 135–144, 2019.

[28] J. Jordan *et al.*, "Turn on switching losses analysis for Si and SiC diodes in induction heating inverters," in *Proc. 13th Eur. Conf. Power Electron. Appl.*, Barcelona, Spain, 2009, pp. 1–9.

[29] J. Kim, S. Kim, W. Oh, and S. Park, "Modeling and analysis of power device losses for induction cooker applications," in *Proc. 21st Int. Conf. Elect. Mach. Syst.*, Jeju, South Korea, 2018, pp. 780–783.

[30] H. Fujita, N. Uchida, and K. Ozaki, "Zone controlled induction heating (ZCIH) a new concept in induction heating," in *Proc. Power Convers. Conf. - Nagoya*, Nagoya, Japan, 2007, pp. 1498–1504.

[31] H. P. Ngoc, H. Fujita, K. Ozaki, and N. Uchida, "Phase angle control of high-frequency resonant currents in a multiple inverter system for zone-control induction heating," *IEEE Trans. Power Electron.*, vol. 26, no. 11, pp. 3357–3366, Nov. 2011.

[32] W. B. Jackson, "Electromagnetic induction heating apparatus for heating elongated metal workpieces," .U.S. Patent 5 510 600, Apr. 23, 1996.

[33] J. I. Rodriguez and S. B. Leeb, "A multilevel inverter topology for inductively coupled power transfer," *IEEE Trans. Power Electron.*, vol. 21, no. 6, pp. 1607–1617, Nov. 2006.

[34] H. N. Pham, H. Fujita, N. Uchida, and K. Ozaki, "Dynamic performance of a current-phase control method for zone-control induction heating systems," in *Proc. IEEE Energy Convers. Congr. Expo.*, San Jose, CA, USA, 2009, pp. 833–839.

[35] H. N. Pham, H. Fujita, N. Uchida, and K. Ozaki, "Analysis and control of the heat distribution in a zone-control induction heating system," in *Proc. Int. Power Electron. Conf.*, Chennai, India, 2010, pp. 2324–2330.

[36] A. M. Green, "Operation of inverters supplying mutually coupled induction heating loads," in *Proc. IEE Colloq. Electromagn. Induction Heating*, 1996, pp. 4/1–4/3.

[37] F. Forest, S. Faucher, J. Gaspard, D. Montloup, J. Huselstein, and C. Joubert, "Frequency-Synchronized resonant converters for the supply of multiwinding coils in induction cooking appliances," *IEEE Trans. Ind. Electron.*, vol. 54, no. 1, pp. 441–452, Feb. 2007.

[38] *Safety Standards for Household Electrical Products*, IEC 60335-2-9, Geneva, Switzerland, 2019.

[39] *Limitation of Voltage Fluctuations and Flicker in Low-Voltage Supply Systems for Equipment With Rated Current 16 A*, IEC Standard 1000-3-3, 1994.

[40] O. Lucia, J. M. Burdio, I. Millan, J. Acero, and D. Puyal, "Load-Adaptive control algorithm of half-bridge series resonant inverter for domestic induction heating," *IEEE Trans. Ind. Electron.*, vol. 56, no. 8, pp. 3106–3116, Aug. 2009, doi: 10.1109/TIE.2009.2022516.

**Eunsu Jang** (Student Member, IEEE) received the B.S degree in electrical engineering from Chosun University, Gwangju, South Korea, in 2016. He has been working toward the combined M.S. and Ph.D. degrees in electrical engineering with Sungkyunkwan University, Seoul, South Korea, since 2016.

His research interests include induction heating, high frequency resonant inverter, and PCS for home appliance.

**Man Jae Kwon** (Student Member, IEEE) received the B.S. degree in information and communications engineering from Myongji University, Yongin, South Korea, in 2019. He is currently working toward the combined M.S. and Ph.D. degrees in electrical engineering from Sungkyunkwan University, Suwon, South Korea.

His current research interests include induction heating, ac/dc converter, and PCS for home appliances.

**Sang Min Park** received the B.S degree from Pukyong National University, Busan, South Korea, in 2014, and the M.S. and Ph.D. degrees from the Sungkyunkwan University, Suwon, Korea, in 2016 and 2020, respectively, all in electrical engineering.

Since 2020, he has been a Senior Research Engineer with Korea Electronics Technology Institute (KETI), Bucheon, South Korea. His current research interests include high-frequency power conversion with wide bandgap devices, on-board chargers and wireless power transfer chargers for electric vehicles, induction heating systems, dc–dc converters for renewable energy, and battery charger for home appliances.

**Hyo Min Ahn** (Member, IEEE) received the B.S, M.S., and Ph.D. degrees in electrical engineering from the Sungkyunkwan University, Suwon, South Korea, in 2014, 2016, and 2020 respectively.

He was with the Digital Appliance Business at Samsung Electronics, Suwon, South Korea, in 2020. His research interests include grid-connected inverters for ESS, high-frequency resonant inverters, and PCS for home appliances.

**Byoung Kuk Lee** (Senior Member, IEEE) received the B.S. and M.S. degrees from Hanyang University, Seoul, South Korea, in 1994 and 1996, respectively, and the Ph.D. degree from Texas A&M University, College Station, TX, USA, in 2001, all in electrical engineering.

From 2003 to 2005, he was a Senior Researcher with Power Electronics Group, Korea Electrotechnology Research Institute, Changwon, South Korea. Since 2006, he has been with the College of Information and Communication Engineering, Sungkyunkwan University, Suwon-si, South Korea. His research interests include on-board chargers and wireless power transfer chargers for electric vehicles, battery management system algorithms, energy storage systems, hybrid renewable energy systems, induction heating cookers for home appliances, modeling and simulation, and power electronics.

Dr. Lee was listed on the 2008 edition of Who's Who in America and the 2009 edition of Who's Who in the World. He is the Guest Associate Editor for the IEEE TRANSACTIONS ON POWER ELECTRONICS, Associate Editor for the IEEE TRANSACTIONS ON TRANSPORTATION ELECTRIFICATION, and Editorial Board Member of the ENERGIES. He was the Presenter for the Professional Education Seminar on the topic On-Board Charger Technology for EVs and PHEVs at the IEEE Applied Power Electronics Conference in 2014. He was also the General Chair for the IEEE Vehicular Power and Propulsion Conference in 2012. From 2016 to 2021, he was a Member of the IEC Conformity Assessment Board.